Invited Review

Dynamic Contrast-Enhanced MRI in Clinical Oncology: Current Status and Future Directions

Anwar R. Padhani, MB, BS*

Dynamic contrast-enhanced magnetic resonance imaging (DCE-MRI) is performed after the administration of intravenous contrast medium to noninvasively access tumor vascular characteristics. DCE-MRI techniques utilizing low-molecular-weight contrast media have successfully made the transition from methodological development to preclinical and clinical validation and are now rapidly becoming mainstream clinical tools. DCE-MRI using macromolecular contrast medium (MMCM) can also assay microvascular characteristics of human tumor xenografts. MMCM approval for human use will occur soon. The success of both techniques depends on their ability to demonstrate quantitative differences of contrast medium behavior in a variety of tissues. Evidence is mounting that kinetic parameters correlate with immunohistochemical surrogates of tumor angiogenesis, including microvessel density, and with pathologic tumor grade. DCE-MRI is being applied to monitor the clinical effectiveness of a variety of treatments, including antiangiogenic drugs. Kinetic parameter changes following treatment have correlated with histopathological outcome and patient survival. This article reviews the current clinical status of low-molecular-weight DCE-MRI and reviews the potential of MMCM techniques for evaluating human tumors. Ongoing challenges faced by DCE-MRI as clinical and research tools will be explored.

Key Words: dynamic contrast-enhanced MRI; angiogenesis; macromolecular contrast media; antiangiogenic drugs; antivascular therapies
J. Magn. Reson. Imaging 2002;16:407–422.

ANGIOGENESIS IS A COMPLEX PROCESS critical to growth and metastasis of malignant tumors. The importance of tumor angiogenesis is well known to clinical oncologists, but until recently has been less familiar to radiologists (1–3). Magnetic resonance imaging (MRI) can be used experimentally to characterize microvasculature, providing information about tumor microvessel structure and function (4–8). MRI techniques can be divided into nonenhanced and contrast media-enhanced methods (9). The latter can be further divided by the type of contrast medium utilized: 1) low-molecular-weight agents (<1000 Da) that rapidly diffuse in the extracellular fluid (ECF) space, 2) large molecular agents (>30,000 Da) designed for prolonged intravascular retention (macromolecular contrast media (MMCM) or blood pool agents), and 3) agents intended to accumulate at sites of concentrated angiogenesis-mediating molecules. Low-molecular-weight contrast agents are in widespread clinical use and are the primary focus of this review. The pathophysiological basis, validation, and quantification of low-molecular-weight dynamic contrast-enhanced MRI (DCE-MRI) will be described, as will current and future clinical applications. MMCM are at the stage of preclinical development and clinical testing; some (ferumoxides) are already available for human use, but angiogenesis assessment is not currently an approved clinical indication. The potential role of macromolecular DCE-MRI for assessing human tumor angiogenesis will be reviewed (8). Molecular targeted contrast media are in preclinical development and are not expected to be approved for human use soon (10).

MRI methods of assessing vascular characteristics have a number of advantages compared with other imaging methods, such as positron emission tomography (PET), computed tomography (CT), ultrasound, or single-photon emission computed tomography (SPECT) (11–13). The signal-to-noise ratio (SNR) and contrast-to-noise ratio (CNR) of MR images are high, and spatial resolution is often equal to that of corresponding morphologic images. MRI is more readily available than PET or xenon inhalation CT. MRI methods are minimally invasive and do not involve radiation exposure. In general, MRI data acquisition is quick and thus can be incorporated into routine patient studies. Importantly, MRI is sensitive to small-vessel function, depending on the technique used, whereas PET is dominated by large-vessel structures. MRI techniques are also sensitive to a variety of contrast mechanisms, including blood flow, microvessel permeability and diameter, tissue oxygenation, and metabolism, which, when taken together, can inform on the tumor microenvironment (Fig. 1). The limitations of MRI techniques are discussed herein.

Paul Strickland Scanner Centre, Mount Vernon Hospital, Middlesex, UK.
*Address reprint requests to: A.R.P., Paul Strickland Scanner Centre, Mount Vernon Hospital, Rickmansworth Road, Northwood, Middlesex HA6 2RN, UK. Email: anwar@padhani.fsnet.co.uk
Received March 12, 2002; Accepted June 19, 2002.
DOI 10.1002/jmri.10176
Published online in Wiley InterScience (www.interscience.wiley.com).

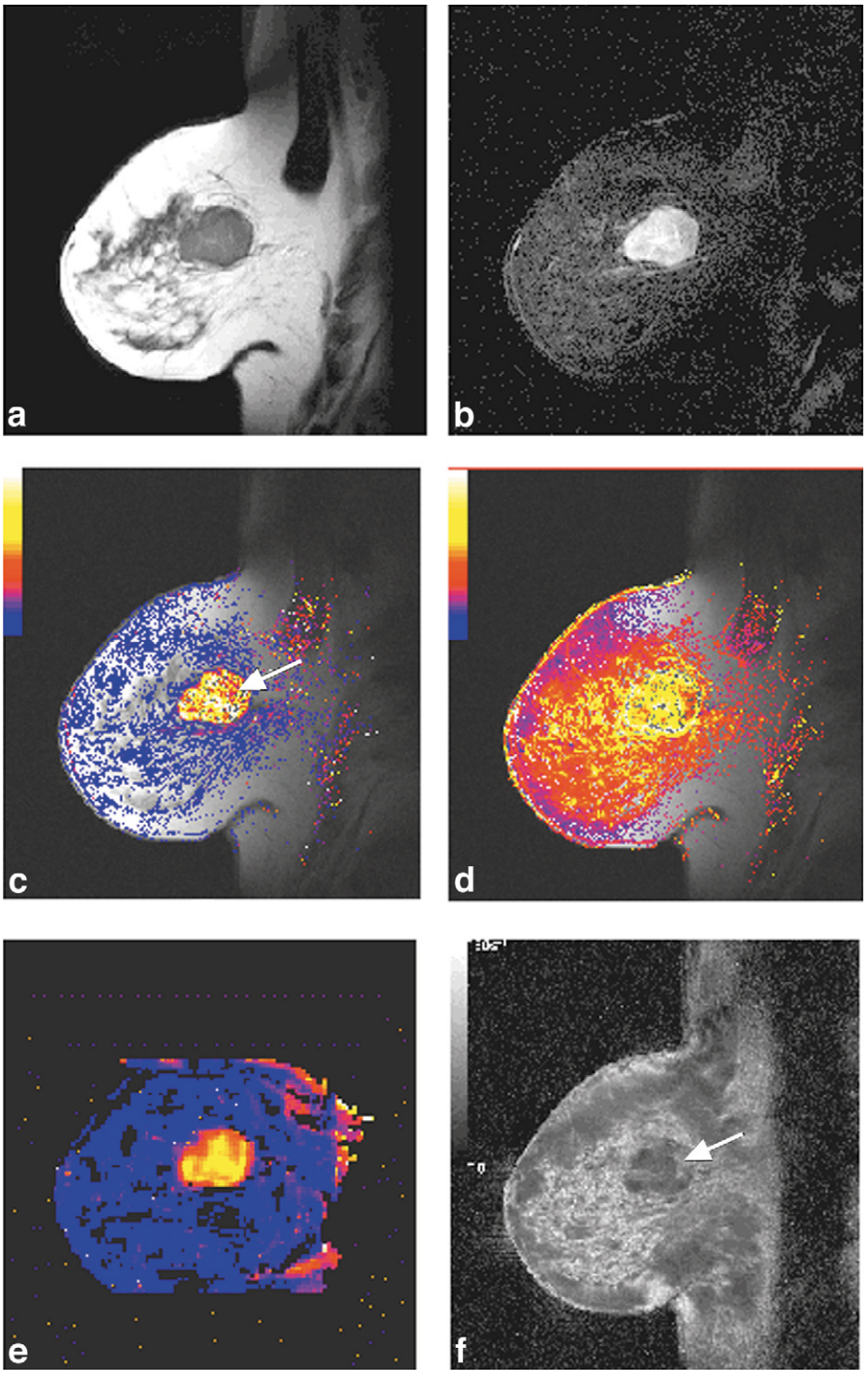

Figure 1. Multifunctional MRI assessment of breast cancer. Images obtained from a 56-year-old woman with invasive ductal breast cancer in a 50-minute examination. **a:** Anatomical, sagittal T2-weighted image of the breast showing a well-defined breast mass compatible with breast cancer. **b:** Early subtraction image obtained 90 seconds after injection of 0.1 mmol/kg of an ECF contrast medium (gadopentetate dimeglumine). **c:** Transfer constant pixel map (maximum transfer constant displayed is 1.0 minute^{-1}). High-transfer constant values, compared to normal breast and heterogeneous distribution, are typical of cancer. There is a focal area of lower-transfer constant posteriorly (arrow). **d:** Leakage space (v_e) pixel map at the same slice position (maximum v_e displayed 100%). There is a large increase in v_e around the tumor such that tumor edges are not identified. **e:** rBV map obtained from a T2*-weighted gradient-echo acquisition using 0.2 mmol/kg of contrast medium. The raw data were obtained at a slightly lower spatial resolution but at the same anatomical location. The tumor is noted to be markedly hypervascular. Note the good spatial correspondence between the rBV image and the transfer constant map (c). **f:** Synthetic R2* maps calculated from a series of gradient-echo images with varying TE (5–75 msec) at the same location. Lighter shades (arrow) of gray posteriorly in the tumor possibly indicate poorer oxygenation or fibrosis. This area corresponds to the tumor region with the lowest blood volume.

CONTRAST AGENT KINETICS

Low-Molecular-Weight ECF Agents

When a bolus of paramagnetic, low-molecular-weight contrast agent passes through a capillary bed, it is transiently confined within the vascular space. This first pass includes the arrival of contrast medium and can last many cardiac cycles. In most tissues except the brain, testes, and retina, the contrast agent rapidly passes into the extravascular-extracellular space (EES), also called leakage space (v_e), at a rate determined by the permeability of the microvessels, their surface area, and blood flow (14–16). In tumors, a variable 12%–45% of the contrast media can leak into the EES during the first pass (17). The transfer constant (K^{trans}) describes the transendothelial transport of a low-molecular-weight contrast medium by diffusion. Three major factors determine the behavior of low-molecular-weight contrast media in tissues: blood perfusion, transport of contrast agent across vessel walls, and diffusion of contrast medium in the interstitial

space. If the delivery of the contrast medium to a tissue is insufficient (flow-limited situations or where vascular permeability is greater than inflow), then blood perfusion will be the dominant factor determining contrast agent kinetics and K^{trans} approximates to tissue blood flow per unit volume (18,19). The latter situation is commonly found in tumors. Note that necrotic regions with a poor blood supply may have low K^{trans} values despite high intrinsic vessel permeability (20,21). If tissue perfusion is sufficient and transport out of the vasculature does not deplete intravascular contrast medium concentration (nonflow limited situations—e.g., in areas of fibrosis or normal brain tissues), then transport across the vessel wall is the major factor that determines contrast medium kinetics. As low-molecular-weight contrast media do not cross cell membranes, their volume of distribution is effectively the interstitial space (v_e). The contrast medium also begins to diffuse into tissue compartments further removed from the vasculature, including areas of necrosis and fibrosis. Over a period typically lasting several minutes to hours, the contrast agent diffuses back into the vasculature (described by the rate constant or k_{ep}) from which it is excreted (usually by the kidneys, although some ECF contrast media have significant hepatic excretion). When capillary permeability is very high, the return of contrast medium is typically quick, resulting in fast washout. Contrast medium elimination from very slow exchange tissues, such as fibrosis and necrosis, occurs slowly, explaining the persistent delayed enhancement characteristic of some tumors, e.g., cholangiocarcinoma and breast cancer (22).

Both T1- and T2*-weighted MRI sequences can be designed to detect the initial vascular phase of contrast medium delivery and thus enable the estimation of tissue perfusion and blood volume. Signal enhancement caused by shortening of T1 relaxation times can be quantified using T1-weighted sequences (23–26). Concentrated intravascular contrast media also produce magnetic field (Bo) inhomogeneities that reduce the signal intensity of surrounding tissues. T2*-weighted sequences can be used to quantify these effects (27,28). T1-weighted sequences are also used to detect the presence of contrast medium in the EES and so can be employed to estimate microvessel permeability surface area product and extracellular leakage space. The analysis methods for evaluating these techniques have their foundations in basic physiology and pharmacology (14,29,30).

Macromolecular Weight Contrast Media

ECF contrast agents have a high first-pass extraction fraction in both normal and abnormal tissues (17). Physiologists have noted that microvessels of cancers are specifically hyperpermeable to macromolecules (31,32). MMCM have molecular sizes that approximate some serum proteins and a minimal single-pass extraction fraction in normal vessels, and therefore appear well suited for the measurement of tumor macromolecular hyperpermeability (17,33,34). MMCM are probably delivered to the interstitial space by nonspecific vesicular transport (vesiculo-vacuolar organelles) or through transendothelial channels (35). Albumin-$(Gd\text{-}DTPA)_{30}$ is the prototype MMCM (70–90 kDa), but this agent has been found to be immunogenic and has significant retention in the liver and bone (36). Polylysine-(Gd-DTPA) is not readily biodegradable, which also makes it unsuitable for human use. Recently, ultrasmall superparamagnetic iron oxide (USPIO) particles (diameter, 20–30 nm) have been investigated as MMCM (37,38). USPIO MMCM persist in the circulation with half-lives of between 3 and 24 hours, depending on the preparation (39). SNR and degree of enhancement are greater with increasing doses of USPIO contrast medium (37). However, at higher doses, T2* effects can overwhelm the desired T1 enhancement effects in tissues. T2* effects can be marked when vascular densities are high and heterogeneously distributed. T2* effects can be minimized by sequence optimization (40).

T2*-WEIGHTED IMAGING FOLLOWING ECF AGENT ADMINISTRATION

Data Acquisition

Perfusion-weighted images can be obtained with bolus-tracking techniques that monitor the passage of contrast material through a capillary bed (27,28). Bolus injection of the contrast medium is essential to the success of these techniques, and the use of MR-compatible power injectors is recommended. When a bolus of paramagnetic contrast agent passes through a capillary bed, it produces magnetic field (Bo) inhomogeneities that result in a decrease in the signal intensity of surrounding tissues. This effect can be observed with susceptibility-weighted T1- or T2*-weighted sequences, the latter providing greater sensitivity and contrast to perfusion effects. In this context, spin-echo sequences are more sensitive to capillary blood flow than gradient-echo sequences, which incorporate signals from larger vessels (41). The degree of signal loss observed is dependent on the vascular concentration of the contrast agent and microvessel size (42) and density. A linear relationship between blood concentration of the contrast agent and change in transverse relaxation time is usually assumed. The SNR of such images can be improved by using higher doses of contrast medium (i.e., $\geq$0.2 mmol/kg of body weight) (43). MRI systems capable of rapid image acquisition are required to adequately characterize these effects. High-specification, echo-planar capable systems are well suited to this task, allowing rapid, multislice acquisition, particularly in brain applications. However, such studies are possible on conventional MRI systems using standard gradient-echo techniques but are limited to fewer slices.

Quantification

Tracer kinetic principles can be used to provide estimates of relative blood volume (rBV), relative blood flow (rBF), and mean transit time (MTT) derived from the first pass of the contrast agent through the microcirculation (27,28,44). Kinetic parameters can be obtained from the integral of the time susceptibility curve or by the fitting of a gamma-variate function to eliminate tracer recirculation effects. These variables are related

by the central volume theorem equation (BF = BV/MTT), but a number of conditions of the central volume theorem are not met. For example, injection time is not instantaneous (in general, not obtainable in biological tissues), and as the arterial input function is not typically measured, these parameters are qualitative or relative. Quantification of these parameters has been undertaken by simultaneous monitoring of the concentration of contrast agent in a large neck or brain vessel (45), and quantified perfusion parameters in normal brain and low-grade gliomas have been obtained (46,47).

Limitations

Limitations specific to T2* MRI methods are discussed here, and those related to DCE-MRI techniques in general are discussed later (vide infra). Contrast recirculation can impair the calculation of perfusion information when integration methods are used. These effects can be minimized by gamma-variate fitting routines. Physiological factors that hinder accurate perfusion measurements include nonlaminar flow, which arises from the presence of irregular caliber vessels; nondichotomous branching; high microvessel permeability, leading to increased blood viscosity from hemoconcentration; and high interstitial pressure. In addition, factors such as machine stability, patient motion, and intrinsic patient variables, particularly cardiac output and upstream stenoses, can affect computations.

The quantification techniques described above only provide accurate measurements of perfusion parameters in the brain because the intact blood-brain barrier (BBB) retains the contrast medium within the vasculature. Errors are introduced if there is marked capillary leakage. This loss of compartmentalization and the T1-enhancing effects of ECF agents in the EES can counter T2* signal-lowering effects, resulting in falsely lowered blood volume computations. Solutions for obtaining more reliable perfusion data under these circumstances are currently being investigated. In areas of moderate BBB breakdown, model-based corrections to the data can be performed to take into account the relative contribution of T1 and T2* components in DCE-MRI studies (48–50). Optimization of pulse sequence parameters to minimize T1 effects can also be used (51). Additionally, predosing with a small amount of contrast medium can be used; this allows T1 shortening effects to occur before the arrival of the main bolus of contrast medium and thus minimize competing T1 and T2* effects. The latter enables rBV to be estimated in visceral tumors, as illustrated in Fig. 1. Another approach is to use non-gadolinium-based susceptibility contrast agents. Dysprosium-based contrast media have a strong T2* effect, but a weak T1 effect, compared to gadolinium chelates (52). Preliminary results indicate that dysprosium-based relative cerebral blood volume (rCBV) maps are superior to those obtained with gadolinium chelates (53,54). USPIO particles designed for bolus injection can be used as susceptibility contrast agents to study tissue perfusion (55,56). Encouraging early clinical results using USPIO particles are beginning to appear in the literature (57,58).

Clinical Experience

Qualitative observations of signal loss were observed on T2*-weighted sequences after gadolinium contrast media were used in clinical studies to characterize liver, breast, and brain tumors. Ichikawa et al were able to discriminate between liver metastases, hemangiomata, and hepatomas on the basis of characteristic signal intensity changes on echo-planar MRI (59). They observed that hemangiomata and hepatomas caused the strongest decreases in signal intensity, but noted that this phenomenon was of shorter duration in hepatomas. These observations are explained by the size and speed of clearance of vascular pools in hemangiomata (large vascular pools with slow clearance) and hepatomas (smaller vessels with fast clearance). Similar observations have been noted after USPIO particle administration for characterizing liver lesions (60). Both Kuhl et al and Kvistad et al have evaluated the value of T2*-weighted imaging after ECF contrast agent administration for characterizing breast lesions (61,62). Both studies showed strong decreases in signal intensity in malignant tissues, whereas susceptibility effects in fibroadenomas were minor. The latter studies showed that it was possible to differentiate carcinomas from fibroadenomas with high specificity using T2*-weighted characteristics despite significant overlap in T1 enhancement patterns. The pathophysiological explanation probably relates to differences in microvessel arrangements, density, and size in malignant tumors and fibroadenomas. A recent histopathological study compared microvessel distributions in invasive breast cancer and fibroadenomas (63). This study demonstrated that there was complete overlap in microvessel density (MVD) counts, but noted that the distribution of microvessels was distinctive. Microvessel distribution in breast carcinomas showed marked regional variations, with fewer vessels seen within the center of tumors than in the periphery. Other investigators have also shown MVD hot spots in breast cancers (64,65). In contradistinction, microvessel distributions in fibroadenomas are more evenly spread within the stroma. Both Kuhl et al and Kvistad et al commented that T2* effects occurred in focal areas that may correspond to the hot spots in MVD counts in tumors.

Quantitative imaging is currently most reliable for normal brain and nonenhancing brain lesions because the contrast medium is retained within the intravascular space. T2*-weighted perfusion mapping techniques have progressively entered neurological practice (66–71). Clinical applications include characterization of tumor vascularity (49,66,70,72), follow-up of treatment response (47,67,71,73), and the study of stroke (74). In the World Health Organization (WHO) grading system for cerebral neoplasms, neovascularization, cellular and nuclear pleomorphism cell density, and necrosis are key histological features (75). Given that MVD is a prognostic feature for astroglial tumors (76), there is a paucity of data correlating T2* kinetic parameters with MVD in human brain tumors. Areas of high tumor rCBV are readily visible in patients with brain gliomas (Fig. 2) (70,77) and appear to correlate with mitotic activity (information on tumor grade) and vascularity,

but not with cellular atypia, endothelial proliferation, necrosis, or cellularity (70). rCBV maps appear to have a high negative predictive value in excluding the presence of high-grade tumor in untreated patients regardless of their enhancement characteristics on T1-weighted MRI. In low-grade gliomas, homogeneous low rCBV is found, whereas higher-grade tumors display both low and high rCBV components (78). rCBV can be used to direct stereotactic biopsy (79,80). This is important because both treatment and prognosis of astroglial tumors are determined by histological grade, and up to 25% of stereotactic brain biopsies are undergraded, compared with resection specimens (81). Other potential uses of T2*-weighted imaging in patients with brain tumors include distinguishing radiation necrosis from recurrent disease (54), determining prognosis (82), and monitoring response to radiotherapy (83) and combination chemotherapy with antiangiogenic drugs (84).

T1-WEIGHTED IMAGING FOLLOWING ECF CONTRAST AGENT ADMINISTRATION

Data Acquisition

T1 relaxation time shortening caused by the contrast medium in the vascular and EES is the mechanism of tissue enhancement observed on T1-weighted images. The degree of signal enhancement is dependent on a number of physiological and physical factors. Physiological factors, which include tissue perfusion, capillary permeability, and volume of the extracellular leakage space, are the parameters of interest in these experiments. Physical factors that determine contrast enhancement include contrast agent dose and method of administration, native T1 relaxation times of the tissue, imaging sequence used, and machine scaling factors (85,86). A discussion of contrast medium dose and methods of administration can be found in the section entitled "Challenges for DCE-MRI Techniques" (vide infra). To monitor the tissue-enhancing effects of ECF agents on T1-weighted images, confounding T2 and T2* effects must be controlled. T1-weighted gradient-echo saturation recovery/inversion recovery snapshot sequences (e.g., turboFLASH) or echo-planar sequences are typically used. Each of these techniques enables the tissue T1 relaxation time to be estimated, and thus allows quantification of contrast medium concentration (87–89). The choice of sequence and parameters used is dependent on intrinsic advantages and disadvantages of the sequences, taking into account T1 sensitivity, anatomical coverage, acquisition times, susceptibility to artifacts arising from magnetic field inhomogeneities, and accuracy for quantification. In order to model tissue contrast behavior (vide infra), the contrast agent concentration at each time point during the imaging procedure needs to be known. Many workers assume that the change in signal intensity or relative signal intensity is directly proportional to the tissue contrast concentration using their sequence (90–92). However, when contrast agent concentrations become large (e.g., within vessels), this becomes a poor approximation, because signal intensity varies nonlinearly with contrast agent concentration. Native T1 relaxation time, choice of flip angle, slice width profiles, and sequence parameter choice may introduce significant errors in these cases (85). If the time-varying T1 relation time can be accurately estimated over a large range of T1 values

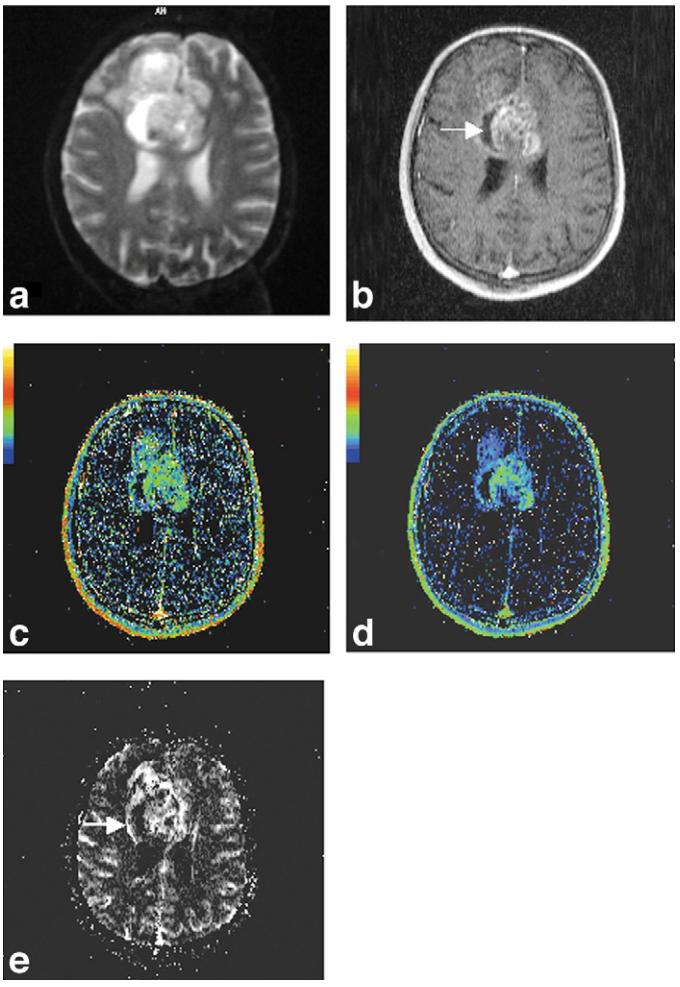

Figure 2. Blood volume and permeability MRI in brain oligodendroglioma. **a:** Axial T2-weighted MR image of a transformed malignant cerebral oligodendroglioma. A large necrotic mass is seen in the frontal lobe extending across the midline. High signal areas within the mass are presumed to represent necrosis. **b:** Gadopentetate dimeglumine (0.2 mmol/kg) enhanced T1-weighted GRE image shows irregular enhancement. A large area of nonenhancement (arrow) is now visible with surrounding edge enhancement. There is little BBB breakdown anteriorly in the tumor. **c:** Transfer constant map (maximum transfer constant displayed = 1 minute^{-1}). The area with the highest transfer constant is in the center of the tumor. There is a region of high transfer constant immediately adjacent to the area of nonenhancement shown in (b). The spatial distribution of transfer constant values does not match the distribution of rCBV (**e**). **d:** Leakage space (v_e) map (maximum v_e demonstrated, 100%). There is a good spatial match of leakage space with transfer constant values. e: rCBV map at the same slice location. The tumor is noted to be markedly hypervascular with a blood volume equal to or greater than cortical gray matter. The blood volume is increased in a heterogeneous manner but appears greatest where enhancement on T1-weighted images is least. For example, the blood volume is least in the immediate vicinity of the large nonenhancing area seen in (b) (arrow).

(89,93,94), then tissue concentration of the contrast agent can be calculated (95).

Quantification

Signal enhancement seen on a dynamic acquisition of T1-weighted images can be assessed in two ways: by the analysis of signal intensity changes (semiquantitative) and by quantifying contrast agent concentration change, or ΔR1, using pharmacokinetic modeling techniques. Semiquantitative parameters describe tissue enhancement using a number of descriptors derived from time-signal intensity curves (96). These parameters include onset time (time from injection to the first increase in tissue signal enhancement), initial and mean gradient of the upsweep of enhancement curves, maximum signal intensity, and washout gradient. Clinical practice has shown that the rate of enhancement is also important for improving the specificity of DCE-MRI, and parameters that include a timing element are widely used (e.g., maximum intensity time ratio (MITR) (97) and maximum focal enhancement at 1 minute (98, 99)). The uptake integral or initial area under the (time signal) curve (AUC) has also been studied (86). Kuhl et al have also successfully correlated the shape of time signal intensity curves with breast lesion histology (100). Semiquantitative parameters have the advantage of being relatively straightforward to calculate, but they have a number of limitations. These limitations include the fact that they do not accurately reflect contrast medium concentration in the tissue of interest and can be influenced by scanner settings (including gain and scaling factors). These factors limit the usefulness of semiquantitative parameters and make between-patient and system comparisons difficult (vide infra). Furthermore, it is often unclear what these parameters reflect physiologically and how robust they are to variations of cardiac output. Evelhoch has suggested that the AUC parameter, when normalized to muscle tissue, parallels K^{trans} estimates over a wide range of tissue input function using mathematical simulations (86). Nevertheless, it is clear that semiquantitative parameters have a close but complex and undefined link to underlying tissue physiology and contrast agent kinetics.

In general, quantitative techniques model tissue contrast agent concentration, although some workers model signal intensity, making the assumption that signal intensity changes are proportional to contrast agent concentration changes (90–92). Signal intensity changes measured during a dynamic enhancement acquisition can be used to estimate contrast agent concentration in vivo (89,93,94). Concentration-time curves are then mathematically fitted using one of a number of recognized pharmacokinetic models, and quantitative modeling parameters are derived. For a detailed discussion on pharmacokinetic modeling techniques, refer to the recent review by Tofts (101). Examples of modeling parameters include the volume transfer constant of the contrast agent (K^{trans}—formally called permeability—surface area product per unit volume of tissue), leakage space as a percentage of unit volume of tissue (v_e), and the rate constant (k_{ep}, also called K_{21}). These standard parameters are related mathematically ($k_{ep} = K^{trans}/v_e$) and recently have been reconciled with others that appear in the literature (19).

Quantitative parameters are more complicated to derive than those derived semiquantitatively, which deters their use at the workbench. The data obtained may not fit the model chosen, and each model makes a number of assumptions that may not be valid for every tissue or tumor type (19,101). Major modeling assumptions include a description of the time-varying blood concentration of contrast agent, also called the input function; the models of Tofts and Brix assume that the supply of contrast medium is not perfusion limited; and some models assume that the tissue blood volume contributes a negligible signal on T1-weighted images, compared with that arising from contrast medium in the interstitial space. Given the proviso that one or more of these assumptions may not be valid, if the contrast agent concentration can be measured accurately and the type, volume, and method of administration are consistent, then it may possible to compare directly pharmacokinetic parameters acquired serially in a given patient and in different patients examined at the same or different scanning sites (102,103). Further discussion of modeling techniques can be found below in the section entitled "Challenges for DCE-MRI Techniques."

Clinical Validation

Histological studies have found that MVD in malignant tissues is higher than in normal parenchyma, but there is an overlap with benign lesions, including inflammatory and proliferative processes (104,105). Many clinical studies have correlated tissue MR enhancement with immunohistochemical MVD measurements (Table 1). Some MRI studies have shown broad correlations between T1 kinetic parameter estimates and MVD (104,106–108), whereas others have found no correlation (109,110). Recently, vascular endothelial growth factor (VEGF), a potent vascular permeability and proangiogenic factor, has been implicated as an additional explanatory factor that determines MR signal enhancement. Knopp et al reported that MR vascular permeability (measured as the efflux rate constant K_{21}) closely correlated with tissue VEGF expression in breast tumors (111). In tumors without significant VEGF expression, a linear correlation of K_{21} and MVD was seen. Once tissue VEGF staining became prominent, K_{21} increased rapidly, independently of MVD. Interestingly, in a careful histological study of cervix cancer, the same group was unable to demonstrate a correlation between the same kinetic parameter and tissue VEGF staining, but was able to demonstrate significant correlations with MVD (112). The importance of VEGF in determining microvascular permeability is supported by the spatial association of hyperpermeable capillaries and VEGF expression in xenografts (113) and by a positive correlation of serum VEGF and rectal cancer transfer constant values, as reported by George et al (114). Furthermore, the observation that treatment with neutralizing anti-VEGF antibodies results in persistent inhibition of albumin-$(GdDTPA)_{30}$ extravasation

Table 1
Validation of Dynamic T1-contrast Enhanced MR Kinetic Parameters With Markers of Angiogenesis in Humans

Author/year	Tumor type	MR parameter	Comparisons with MVD (unless stated) and correlation coefficient (r^2)	Statistical significance level
Buadu et al. [1996](65)	Breast	Steepest slope	0.83	0.001
Stomper et al. [1997](104)	Breast	Maximum amplitude	NS	0.02
Hawighorst et al. [1997, 1998](106, 112)	Cervix	Amplitude, k_{21}	A & MVD - 0.41	< 0.001
			K_{21} & MVD - 0.46	< 0.05
			A & VEGF	NS
			K_{21} & VEGF	NS
Buckley et al. [1997](108)	Breast	Enhancement at 1 minute	0.47	0.002
Hulka et al. [1997](109)	Breast	Extraction flow product	Malignant	0.8
			Benign lesions	0.4
			Malignant and benign lesions 0.36	< 0.01
Tynninen et al. [1999](107)	Brain	Presence or absence of enhancement	NS	0.01
Knopp et al. [1999](111)	Breast	K_{21}	VEGF - 0.52	0.05
			MVD in VEGF positive lesions	NS
			MVD in VEGF negative lesions 0.71	0.07
Ikeda et al. [1999](197)	Breast	K^{trans}	0.89	< 0.01
Cooper et al. [2000](110)	Cervix	Signal intensity increase	0.02	NS
		Rate of signal intensity increase	0.04	NS
George et al. [2001](114)	Rectal	K^{trans}	Serum VEGF 0.48	0.01

NS = not stated; MVD = microvessel density; VEGF = vascular endothelial growth factor.

in xenografts (115) and reductions in kinetic parameters after treatment with VEGF tyrosine kinase inhibitors in humans (116) lends weight to the important role played by VEGF in determining MR enhancement. Other characteristics that have been correlated with enhancement patterns include the degree of stromal cellularity and fibrosis (22,117) and tissue oxygenation (110,118).

Clinical Experience

Analysis of enhancement seen on T1-weighted DCE-MRI has been investigated in a number of clinical situations. Its role in detecting subclinical disease remains to be determined and may include screening of subjects at high genetic risk of breast cancer; the latter application is the subject of several ongoing clinical trials (119–122). A more established role is in lesion characterization, where DCE-MRI has found a role in distinguishing benign from malignant breast and musculoskeletal lesions (98,123). Simple observations from signal intensity time curves have shown that malignant tissues generally enhance early, with rapid and large increases in signal intensity compared with benign tissues, which in general show a slower increase in signal intensity. In the breast this difference is most marked 1–3 minutes after contrast medium administration (97,98,124,125). However, investigators have noted that there is an overlap in the enhancement rates of benign and malignant breast lesions (126–128). As a result, the sensitivity of breast MRI is high, but specificities are more variable, with fibroadenomas in particular demonstrating signal enhancement patterns similar to that of invasive cancer (129). Nonmalignant proliferative tissues such as benign prostatic hyperplasia are also avidly enhancing in a pattern similar to prostate cancer (130–132). Dynamic T1-weighted MRI studies have been found to be of value in the staging of gynecological malignancies and bladder and prostate cancers (132–134). For example, DCE-MRI can improve the accuracy of prostate cancer staging when used in conjunction with T2-weighted images in patients with equivocal capsular penetration or seminal vesicle invasion (132,135).

DCE-MRI is also able to predict or monitor the effects of a variety of treatments. These include neoadjuvant chemotherapy in bladder and breast cancers and bone sarcomas (136–140). In breast cancer, for example, it has recently been shown that a decrease in transendothelial permeability accompanies tumor response to chemotherapy (Fig. 3) and that an early (1 or 2 cycles of treatment) increase or no change in permeability can predict nonresponsiveness (141). Other treatments that can be monitored include radiotherapy in rectal and cervix cancers (114,142–144), androgen deprivation in prostate cancer (139), and vascular embolization of uterine fibroids (145–147). A number of studies have recently reported on the use of T1-weighted DCE-MRI for monitoring the effects of antiangiogenic/antivascular treatments (Fig. 4) (116,148,149). A discussion of the clinical roles for DCE-MRI in evaluating antiangiogenic/antivascular drug treatments can be found below. Response assessment studies show that successful treatment results in a decrease in the rate of enhancement and that poor response results in persistent abnormal enhancement, however judged (semiquantitatively or quantitatively). The lack of specificity for DCE-MRI as a tumor response variable (i.e., it can be affected by most treatments) may reflect on the fact that tumor cell kill, no matter how achieved, ultimately results in vascular compromise. This allows DCE-MRI to be used as an early tumor response variable, but may mean that DCE-MRI is limited in its ability to mecha-

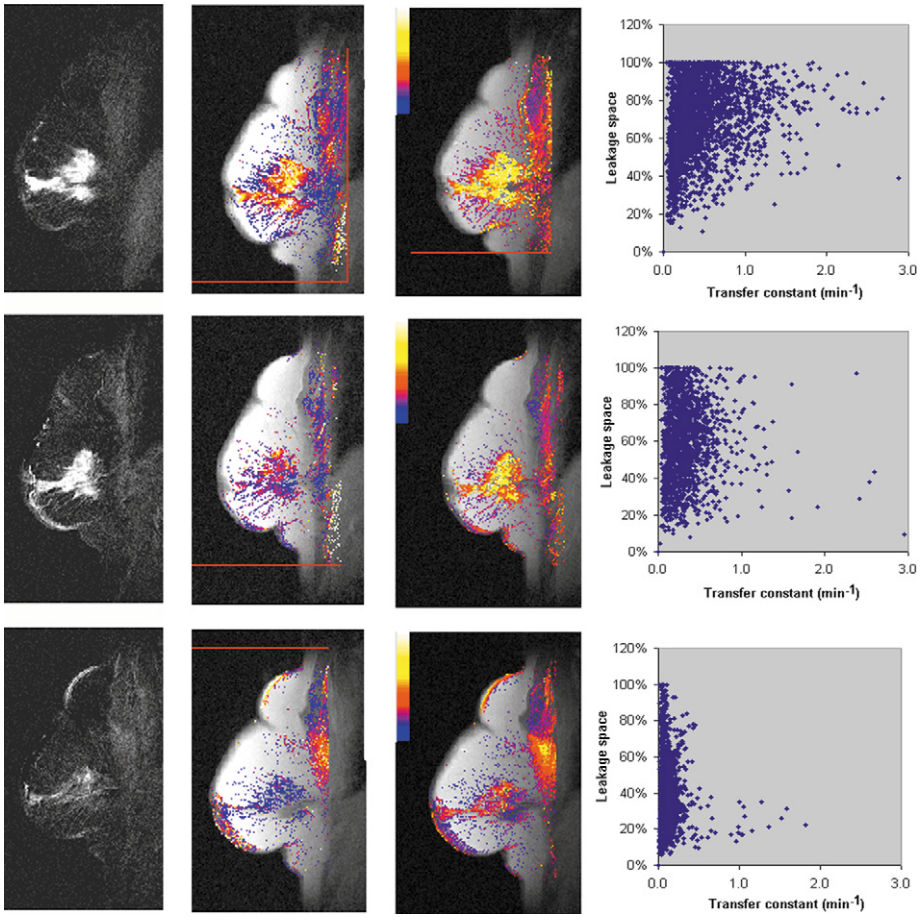

Figure 3. Monitoring chemotherapy response of breast cancer with dynamic MRI. A 58-year-old postmenopausal woman with a recurrent infiltrating ductal carcinoma of the breast. Columns depict anatomic subtraction images (obtained by subtracting MR image acquired at 100 seconds after contrast agent administration from baseline image), corresponding transfer constant maps (color range, 0–1 minute^{-1}), leakage space (maximum v_e value, 100%), and scatter plots showing individual pixel transfer constant and leakage space values. The pixel values displayed are from the whole tumor ROIs in four imaging slices. Scatter plots are amenable to statistical analysis and have the advantage of enabling the changing relationships between kinetic variables to be appreciated. Rows show data before treatment and after two and six courses of 5-fluorouracil, epirubicin, and cyclophosphamide (FEC) chemotherapy. With treatment, a reduction in the number of enhancing pixels is seen (first examination = 4215, second examination = 2080, third examination = 1400). A stepwise reduction in kinetic parameter estimates is seen. Median transfer constant values: first examination = 0.39 minute^{-1}, second examination = 0.28 minute^{-1}, third examination = 0.085 minute^{-1}. Median v_e values: first examination = 72%, second examination = 61%, third examination = 35%.

nistically inform on nonvascular processes that underlie tumor response.

Recently, enhancement parameters have been shown to predict prognosis in patients with cervix cancers; that is, tumors with a fast initial rate of enhancement or vascular permeability were more likely to have a poorer prognosis (150), despite having a higher radiotherapy response rate (151). DCE-MRI studies have also been found to be of value in detecting tumor relapse within treated tissues of the breast and pelvis (125,152–158). For example, in the breast, early and rapid enhancement has been shown to be good at discriminating between scar tissue and recurrent tumor. Many studies now suggest that time since surgery and prior radiotherapy need to be taken into account to avoid errors when evaluating recurrent disease (154,155). Heywang-Kobrunner et al (157), showed that the time interval since treatment completion for breast cancer is important diagnostically. They found that up to 9 months after treatment it was not possible to differentiate between treatment change and recurrent malignancy. Enhancement in the treated breast progressively decreased, and after 18 months, no significant enhancement was seen in most cases of postoperative scarring, whereas enhancement was present with recurrent disease.

IMAGING AFTER MMCM ADMINISTRATION

A timed series of T1-weighted images is used to detect and measure MMCM hyperpermeability. Ideally, both the tumor and the blood pool are monitored simultaneously (34,159). Numerous approaches have been proposed for analysis of the MRI data. Some approaches ignore the input function, while others include the blood response curve to correct for variations in injection speed, contrast elimination, and circulation time. The application of a bidirectional kinetic model to

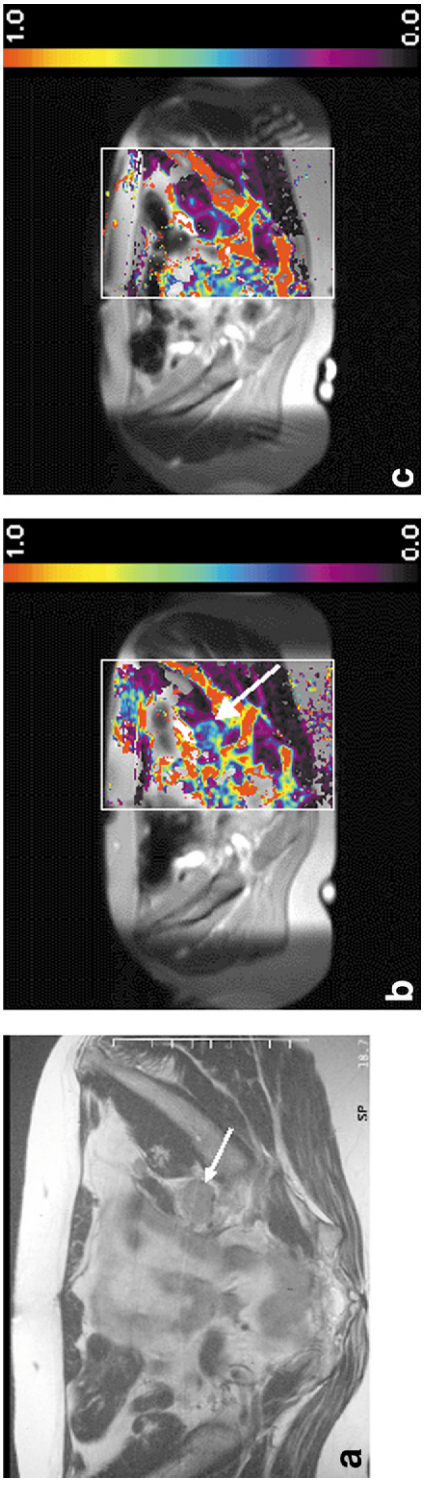

Figure 4. Significant changes in tumor transfer constant following antivascular targeting treatment. **a:** Axial T2-weighted MRI through the midpelvis shows a large, left inferior hypogastric lymph node (arrow) in a patient with malignant peritoneal carcinoma. Transfer constant map (maximum transfer constant displayed 1.0 minute^{-1}) before (**b**) and 4 hours after (**c**) administration of combretastatin (52 mg/m^2). A marked reduction in the transfer constant is seen in the lymph node, particularly in its center.

the dynamic response data enables the estimation of the coefficient of endothelial permeability (K^{PS}) and the fractional plasma volume (fPV) (159,160).

Only preclinical validation of MMCM techniques appears in the literature. An early study using albumin-$(Gd\text{-}DTPA)_{30}$ showed significant hyperpermeability of tumors, compared to normal tissues in a rat fibrosarcoma model (161). Using quantification techniques, van Dijke et al showed a strong positive correlation between tumor K^{PS} and fPV with histological MVD in two subtypes of mammary R3230 adenocarcinoma, one slow growing and the other fast and aggressive (162). Recently, Helbich et al studied the same tumor model using a variety of DCE-MRI techniques with an ECF contrast agent and showed no significant correlations between enhanced parameters (except for T2*-weighted imaging) and histological MVD (163). Intermediate-sized molecules in the range of 15–30 kDa have also been investigated as MMCM, but have shown limitations, including poor correlation with tumor histological grades (164–166). For example, Su et al evaluated three contrast agents of differing molecular weights—Gd-DTPA (<1 kDa), gadomer-17 (35 kDa), and albumin-$(Gd\text{-}DTPA)_{30}$ (70–90 kDa)—to study breast tumors in xenografts (166). They confirmed that Gd-DTPA was able to distinguish benign from malignant tumors, but was unable to grade malignant tumors. They found that gadomer-17 was able to distinguish between high- and low-grade malignant tumors, but was unable to distinguish low-grade cancers from benign lesions. Albumin-$(Gd\text{-}DTPA)_{30}$ was able to distinguish three, but low CNR in the images was a major technical concern. Recently, a study reported on the use of USPIO-enhanced MRI on chemically induced breast tumors and showed that K^{PS} estimates correlated significantly with the histological tumor grade (38). The correlations were essentially the same as those obtained using albumin-$(Gd\text{-}DTPA)_{30}$ in the same tumors (37).

Once approved for human use, MMCM assays of tumor microvascular characteristics may be able to address a number of important clinical issues. These include noninvasive characterization of tumors, particularly at anatomic sites that are difficult to biopsy (e.g., brain tumor grading), and distinguishing of benign, proliferative lesions (e.g., fibroadenoma and benign prostatic hyperplasia) from cancer. A preclinical study has shown that MMCM-enhanced MRI can monitor the antivascular effects of anti-VEGF antibody treatment in xenografts (115). When monoclonal human anti-VEGF antibody was administered to athymic rats implanted with human MB-MDA-435 breast adenocarcinomas, large reductions in permeability were seen within 24 hours of treatment. Reductions in K^{PS} occurred without a change in fPV. This suggests that monitoring antiangiogenic tumor response is another possible clinical application (vide infra).

CHALLENGES FOR DCE-MRI TECHNIQUES

Imaging Protocol Standardization

From the above discussion, it is clear that a variety of MRI techniques can evaluate microvascular structure

and function. This variety can make it difficult to make meaningful comparisons of data obtained from different imaging centers. It is recognized that high resolution and short imaging time are competing examination strategies on current equipment and software. Higher temporal resolution imaging necessitates reduced spatial resolution, decreased anatomic coverage, or a combination thereof. Higher temporal resolution techniques are essential for T2*-weighted techniques and appear to improve specificity of T1-weighted examinations because of better characterization of signal intensity time curves; one study has suggested that characterization of breast lesions is optimal using image acquisition times of 1–2 seconds (124). Even though data collection procedures for quantitative examinations differ from those used in routine clinical practice, there is debate on which technique(s) is best (21,91,103). The imaging community needs to agree on a limited number of examination and analysis protocols in order to enable techniques to be validated for use in clinical trials. Standardized methods for quantified T1-weighted data collection have recently been published (9,167).

The dose and method of administration of contrast agent affect modeling procedures and clinical results. For example, Heywang-Kobrunner et al showed that the accuracy of breast MRI was better using a contrast medium at a dose of 0.16 mmol/kg of body weight (compared to 0.1 mmol/kg) (168). What is not clear is whether a higher contrast medium dose improves examination performance on high- and lower-field-strength systems, with thinner slices, with other pulse sequences and parameters (when T2* effects may become dominant), or when routine subtraction image analysis of dynamic data is performed. A major source of variability in the DCE-MRI literature relates to the method of contrast administration. Typically, contrast agents are given as either a bolus (169) or infusion (90). When a powered injector gives the bolus injection, reproducibility of the injection technique is ensured. Recent work suggests that short injection times are optimal when using fast imaging techniques, especially when evaluating lesions with high microvessel permeability with ECF agents (170,171); conversely, slower infusion methods may be better when the temporal resolution of the study is longer (91). The method of ECF contrast medium administration needs to take into account sequence choice and sensitivity to T2* and T1 effects.

Another issue that needs to be addressed is that of data acquisition and analysis methods in body parts where there is a large degree of physiological movement, such as the lungs and liver. The presence of motion can invalidate parameter estimates. Navigator techniques developed for cardiac MRI may be adapted for moving body organs (172). A related issue is that of data collection in the same imaging plane on repeated examinations. Registration software is not widely available and will be needed for longitudinal functional imaging response studies evaluating novel anticancer drugs.

Quantification

A practical question often asked is whether it is necessary to quantify DCE-MRI data to answer important clinical questions. Simple morphologic and semiquantitative analyses already work well in a number of clinical situations. However, it is important to realize that semiquantitative diagnostic criteria cannot be simply applied from one center to another, particularly when different equipment and sequences are used. For example, it is known that the background or baseline signal for any given tissue will differ by the choice of imager even if identical sequences are used. Thus, the calculation of the degree of enhancement (e.g., as percent signal intensity change from baseline) will differ according to the type of imager used. Consequently, the degree of enhancement that distinguishes one tissue from another on a particular machine type may give erroneous results on another. This has been a real practical problem in the UK multi-intuitional trial evaluating breast MRI for screening women at high genetic risk for breast cancer (120). Quantification techniques aim to minimize such errors while at the same time informing on physiological processes and are therefore preferred when evaluating angiogenic interventions. Quantification techniques rely on the fitting of the data acquired to a mathematical model. Experience shows that the model chosen may not fit the data acquired (modeling failures) and that apparently sensible kinetic values can be obtained even from noisy data. The causes of such modeling failures are complex and often not well understood. Reasons include high vascular permeability (i.e., when the intravascular contrast medium concentration cannot be maintained due to markedly leaky vessels in the setting of limited blood flow), high tissue blood volumes, multiple tissue compartments, and an incorrect or assumed arterial input function. We do not have models that fit all data, and more sophisticated models that provide insights into tissue compartment behavior are needed (24,85,173).

Measurement Error

Repeatability is the variation between measurements of the same quantity on the same individual and informs on equipment variations. Reproducibility measures the typical error between observers and instruments when evaluating the same quantity (appraiser variations). An estimate of measurement error enables us to decide whether a change in observation represents a real change (174–176). Data addressing the precision and measurement variability of DCE-MRI techniques are urgently needed and should be an integral part of any prospective study that evaluates functional response to therapy (177–180). The factors that determine measurement error need to be defined for a given quantitative modeling technique. These include imaging instrumentation and setup procedures, imaging technique, contrast injection protocol, modeling techniques (including assumptions), and arterial input function (AIF). Reliable methods for measuring and incorporating input functions into routine DCE-MRI studies are only now emerging (23,181). The effect of the AIF on kinetic parameter estimates can be evaluated by using math-

ematical simulations (182) and has recently been shown to improve the reproducibility of kinetic parameter estimates (181).

Validation

Any imaging assay of tumor microvascular characteristics must be rigorously validated against accepted surrogates of angiogenesis and other physiological parameters. Unfortunately, no single imaging assay or surrogate may be adequate to reflect the whole spectrum of events involved in angiogenesis. Commonly used and appropriate surrogates include histological MVD, as counted on factor VIII, or CD34-stained tumor specimens and vascular maturation index (VMI) (9,183). Also, quantitative measures of VEGF or other known mediators of angiogenesis, in the tumor tissue itself or in the plasma, can be compared to the imaging assay results (111,114,150). Similarly, DCE-MRI techniques should be validated against other techniques that measure vascular function (184–187).

Data Presentation and Heterogeneity

Analysis and presentation of imaging data needs to take into account the heterogeneity of tumor vascular characteristics. Analysis methods and presentation of DCE-MRI data varies in the literature. Most dynamic MRI studies utilize user-defined regions of interest (ROIs). ROI methods yield graphical outputs with good SNR, but lack spatial resolution and are prone to partial volume averaging errors. In its simplest form, an ROI encompassing the whole tumor is drawn from which an average enhancement curve is extracted. This method also ignores heterogeneity of tumor enhancement by assuming that the averaged kinetic parameter estimate equates to those that would be obtained from individual pixels. Recently, Hayes et al have shown that this is a close approximation (188). However, many authors have commented that whole tumor ROI assessment may be inappropriate, particularly for the evaluation of malignant lesions where heterogeneous areas of enhancement are diagnostically important (70,89,99). Therefore, selective sampling of regions within a tumor is used by most researchers, based on the premise that the discrimination of lesions is improved by selective sampling (189).

Another approach of displaying dynamic data is by pixel mapping. This method depicts kinetic enhancement information as maps exactly co-registered with anatomical images on a pixel-by-pixel basis. This type of display has a number of advantages, including the appreciation of heterogeneity of enhancement and removal of the need for selective place of user-defined ROIs. The risk of missing important diagnostic information and of creating ROIs that contain more than one tissue type is reduced. An important advantage is being able to spatially match tumor vascular characteristics such as blood volume, blood flow, permeability, and leakage space. Differences in the distributions of kinetic parameters have been shown in xenografts (113) and human tumors (190–192) (Figs. 1 and 2). Such displays provide unique incites of tumor structure, function, and response. Pixel mapping techniques have the disadvantages of having poor SNRs, requiring specialist software for their generation (23,91,96). Although visual appreciation of heterogeneity is improved by pixel mapping displays, quantification of the same can be more difficult. Recently, histogram analysis has been used to quantify the heterogeneity of tumors for comparative and longitudinal studies, for monitoring the effects of treatment, and to show the regression or development of angiogenic hot spots (144,188). Pixel scatter plots of co-registered multifunctional parameters can also be used to display heterogeneity and have the advantage of enabling relationships between kinetic variables to be appreciated when assessing response (192) (Fig. 3).

Impact on Current and Future Clinical Practice

The data presented in this review show the potential utility of DCE-MRI techniques in a variety of clinical situations. Most clinical studies to date have been performed in selected (usually small) patient groups, and more studies with sufficient power are needed to address specific clinical problems where a potential role has been shown. Examples of such studies include screening women at high genetic risk of breast cancer (119–122) and comprehensive staging of breast cancer (193,194).

DCE-MRI techniques will play an important role in the functional assessment of patients treated by antiangiogenic/antivascular therapies (195). Antiangiogenic drugs prevent the formation of neovasculature and thus require continuous treatment, inducing long-term changes in the vasculature. Early drug trials have reported very low toxicity compared with chemotherapy. In contrast, vascular-targeting drugs cause rapid vascular damage that can result in hemorrhagic necrosis of tumors. Their effect on vasculature is reversible often within hours of a single treatment and thus requires intermittent administration. Early drug trials have shown that vascular-targeting drugs have significant toxicity. DCE-MRI should be able to address a number of important issues with regard to the use of such treatments, including the category of medication to be used, dose optimization based on the suppression of a specific kinetic parameter, early detection of response, and impact of treatment on the tumor vasculature.

The number of antiangiogenic/antivascular compounds entering clinical trials is rapidly increasing; each is aimed at different points in the angiogenesis and metastatic cascade. The efficacy of treatment could vary between tumors, and thus the choice of optimal treatment will require information on the biology and functional status of the tumor vasculature. Noninvasive characterization of the angiogenic status of specific tumors may allow rational selection of such treatments. Since antiangiogenic treatments have lower toxicity than antivascular treatments and chemotherapy, toxicity-based selection of the dose may not be appropriate. The biologically active dose can be defined by DCE-MRI by showing quantitative biological effects specified by a mechanism-based knowledge of drug action

(116,148,149). The intrinsic redundancy of signaling mechanisms associated with angiogenesis will lead to partial or complete resistance of the tumor vessels to therapy. Interest in imaging techniques that can provide early indicators of effectiveness at a functional or molecular level has therefore increased. Tumor response to treatment can be detected by imaging techniques that are capable of monitoring changes in perfusion, blood volume, or microvessel permeability. Finally, monitoring the therapeutic effects of antiangiogenic therapy is expected to be harder to detect and quantify. This is because antiangiogenic treatments may not result in substantial reductions in tumor volume and conventional size measurements of response may be insensitive or markedly delayed even when there is a significant biological effect. Imaging-based approaches will therefore also be valuable for monitoring long-term treatment.

CONCLUSIONS

There are definite clinical needs to develop non-invasive imaging assays of tumor angiogenesis. DCE-MRI is the only one of a number of MRI techniques that can evaluate tumors with respect to their state of the functional microcirculation. DCE-MRI techniques using ECF agents are far from ideal in this regard, and MMCM may well prove superior in the long term. There are a number of challenges that must be met before these techniques can become mainstream diagnostic and research tools. These imaging techniques will have widespread clinical applications and a central role in the evaluation of novel therapies, for example, antiangiogenesis drugs and gene and antibody therapies (196). Given the lead time between the development of a new therapeutic approach or drug in the laboratory and its evaluation in the clinic, radiologists need to evaluate fully currently available and new imaging methods for assessing tumor microvascular function.

ACKNOWLEDGMENTS

The support of Cancer Research UK and the Childwick Trust, who respectively support the work of the Clinical Magnetic Resonance Research Group at the Royal Marsden Hospital and at the Paul Strickland Scanner Centre, UK is gratefully acknowledged.

REFERENCES

1. Folkman J, Beckner K. Angiogenesis imaging. Acad Radiol 2000; 7:783–785.
2. Li WW. Tumor angiogenesis: molecular pathology, therapeutic targeting, and imaging. Acad Radiol 2000;7:800–811.
3. Passe TJ, Bluemke DA, Siegelman SS. Tumour angiogenesis: tutorial on implications for imaging. Radiology 1997;7:593–600.
4. Neeman M. Preclinical MRI experience in imaging angiogenesis. Cancer Metastasis Rev 2000;19:39–43.
5. Bhujwalla ZM, Artemov D, Glockner J. Tumor angiogenesis, vascularization, and contrast-enhanced magnetic resonance imaging. Top Magn Reson Imaging 1999;10:92–103.
6. Gillies RJ, Bhujwalla ZM, Evelhoch J, et al. Applications of magnetic resonance in model systems: tumor biology and physiology. Neoplasia 2000;2:139–151.
7. Neeman M, Provenzale JM, Dewhirst MW. Magnetic resonance imaging applications in the evaluation of tumor angiogenesis. Semin Radiat Oncol 2001;11:70–82.
8. Brasch R, Turetschek K. MRI characterization of tumors and grading angiogenesis using macromolecular contrast media: status report. Eur J Radiol 2000;34:148–155.
9. Brasch RC, Li KC, Husband JE, et al. In vivo monitoring of tumor angiogenesis with MR imaging. Acad Radiol 2000;7:812–823.
10. Weissleder R, Mahmood U. Molecular imaging. Radiology 2001; 219:316–333.
11. Blankenberg FG, Eckelman WC, Strauss HW, et al. Role of radionuclide imaging in trials of antiangiogenic therapy. Acad Radiol 2000;7:851–867.
12. Miles KA. Dynamic contrast enhanced MR. Clin Radiol 1996;51: 78–79.
13. Ferrara KW, Merritt CR, Burns PN, Foster FS, Mattrey RF, Wickline SA. Evaluation of tumor angiogenesis with US: imaging, Doppler, and contrast agents. Acad Radiol 2000;7:824–839.
14. Crone C. The permeability of capillaries in various organs as determined by the use of 'indicator diffusion' method. Acta Physiol Scand 1963;58:292–305.
15. Yuh WT. An exciting and challenging role for the advanced contrast MR imaging. J Magn Reson Imaging 1999;10:221–222.
16. Taylor JS, Reddick WE. Evolution from empirical dynamic contrast-enhanced magnetic resonance imaging to pharmacokinetic MRI. Adv Drug Deliv Rev 2000;41:91–110.
17. Daldrup HE, Shames DM, Husseini W, Wendland MF, Okuhata Y, Brasch RC. Quantification of the extraction fraction for gadopentetate across breast cancer capillaries. Magn Reson Med 1998; 40:537–543.
18. Taylor JS, Tofts PS, Port R, et al. MR imaging of tumor microcirculation: promise for the new millennium. J Magn Reson Imaging 1999;10:903–907.
19. Tofts PS, Brix G, Buckley DL, et al. Estimating kinetic parameters from dynamic contrast-enhanced T(1)-weighted MRI of a diffusable tracer: standardized quantities and symbols. J Magn Reson Imaging 1999;10:223–232.
20. Su MY, Jao JC, Nalcioglu O. Measurement of vascular volume fraction and blood-tissue permeability constants with a pharmacokinetic model: studies in rat muscle tumors with dynamic Gd-DTPA enhanced MRI. Magn Reson Med 1994;32:714–724.
21. Degani H, Gusis V, Weinstein D, Fields S, Strano S. Mapping pathophysiological features of breast tumors by MRI at high spatial resolution. Nat Med 1997;3:780–782.
22. Matsubayashi R, Matsuo Y, Edakuni G, Satoh T, Tokunaga O, Kudo S. Breast masses with peripheral rim enhancement on dynamic contrast-enhanced MR images: correlation of MR findings with histologic features and expression of growth factors. Radiology 2000;217:841–848.
23. Li KL, Zhu XP, Waterton J, Jackson A. Improved 3D quantitative mapping of blood volume and endothelial permeability in brain tumors. J Magn Reson Imaging 2000;12:347–357.
24. Ludemann L, Hamm B, Zimmer C. Pharmacokinetic analysis of glioma compartments with dynamic Gd-DTPA-enhanced magnetic resonance imaging. Magn Reson Imaging 2000;18:1201–1214.
25. Hacklander T, Hofer M, Reichenbach JR, Rascher K, Furst G, Modder U. Cerebral blood volume maps with dynamic contrast-enhanced T1-weighted FLASH imaging: normal values and preliminary clinical results. J Comput Assist Tomogr 1996;20:532–539.
26. Hacklander T, Reichenbach JR, Hofer M, Modder U. Measurement of cerebral blood volume via the relaxing effect of low-dose gadopentetate dimeglumine during bolus transit. AJNR Am J Neuroradiol 1996;17:821–830.
27. Barbier EL, Lamalle L, Decorps M. Methodology of brain perfusion imaging. J Magn Reson Imaging 2001;13:496–520.
28. Sorensen AG, Tievsky AL, Ostergaard L, Weisskoff RM, Rosen BR. Contrast agents in functional MR imaging. J Magn Reson Imaging 1997;7:47–55.
29. Zierler KL. Theory of use of indicators to measure blood flow and extracellular volume and calculation of trans capillary movement of tracers. Circulation Res 1963;12:464–471.
30. Kety SS. The theory and applications of the exchange of inert gas at the lungs and tissues. Pharmacol Rev 1951;3:1–41.
31. Jain RK. Transport of molecules across tumor vasculature. Cancer Metastasis Rev 1987;6:559–593.

32. Gerlowski LE, Jain RK. Microvascular permeability of normal and neoplastic tissues. Microvasc Res 1986;31:288–305.
33. Su MY, Muhler A, Lao X, Nalcioglu O. Tumor characterization with dynamic contrast-enhanced MRI using MR contrast agents of various molecular weights. Magn Reson Med 1998;39:259–269.
34. Roberts TP, Roberts HC, Brasch RC. Optimizing imaging techniques to reduce errors in microvascular quantitation with macromolecular MR contrast agents. Acad Radiol 1998;5(Suppl 1): S133–S136.
35. Dvorak AM, MacGlashan Jr DW, Morgan ES, Lichtenstein LM. Vesicular transport of histamine in stimulated human basophils. Blood 1996;88:4090–4101.
36. Schmiedl U, Ogan M, Paajanen H, et al. Albumin labeled with Gd-DTPA as an intravascular, blood pool-enhancing agent for MR imaging: biodistribution and imaging studies. Radiology 1987; 162:205–210.
37. Turetschek K, Roberts TP, Floyd E, et al. Tumor microvascular characterization using ultrasmall superparamagnetic iron oxide particles (USPIO) in an experimental breast cancer model. J Magn Reson Imaging 2001;13:882–888.
38. Turetschek K, Huber S, Floyd E, et al. MR imaging characterization of microvessels in experimental breast tumors by using a particulate contrast agent with histopathologic correlation. Radiology 2001;218:562–569.
39. Wang YX, Hussain SM, Krestin GP. Superparamagnetic iron oxide contrast agents: physicochemical characteristics and applications in MR imaging. Eur Radiol 2001;11:2319–2331.
40. Bremerich J, Roberts TP, Wendland MF, et al. Three-dimensional MR imaging of pulmonary vessels and parenchyma with NC100150 injection (Clariscan). J Magn Reson Imaging 2000;11: 622–628.
41. Simonsen CZ, Ostergaard L, Smith DF, Vestergaard-Poulsen P, Gyldensted C. Comparison of gradient- and spin-echo imaging: CBF, CBV, and MTT measurements by bolus tracking. J Magn Reson Imaging 2000;12:411–416.
42. Dennie J, Mandeville JB, Boxerman JL, Packard SD, Rosen BR, Weisskoff RM. NMR imaging of changes in vascular morphology due to tumor angiogenesis. Magn Reson Med 1998;40:793–799.
43. Bruening R, Berchtenbreiter C, Holzknecht N, et al. Effects of three different doses of a bolus injection of gadodiamide: assessment of regional cerebral blood volume maps in a blinded reader study. AJNR Am J Neuroradiol 2000;21:1603–1610.
44. Rosen BR, Belliveau JW, Buchbinder BR, et al. Contrast agents and cerebral hemodynamics. Magn Reson Med 1991;19:285–292.
45. Rempp KA, Brix G, Wenz F, Becker CR, Guckel F, Lorenz WJ. Quantification of regional cerebral blood flow and volume with dynamic susceptibility contrast-enhanced MR imaging. Radiology 1994;193:637–641.
46. Wenz F, Rempp K, Brix G, et al. Age dependency of the regional cerebral blood volume (rCBV) measured with dynamic susceptibility contrast MR imaging (DSC). Magn Reson Imaging 1996;14: 157–162.
47. Wenz F, Rempp K, Hess T, et al. Effect of radiation on blood volume in low-grade astrocytomas and normal brain tissue: quantification with dynamic susceptibility contrast MR imaging. AJR Am J Roentgenol 1996;166:187–193.
48. Kuperman VY, Alley MT. Differentiation between the effects of T1 and T2* shortening in contrast-enhanced MRI of the breast. J Magn Reson Imaging 1999;9:172–176.
49. Barbier EL, den Boer JA, Peters AR, Rozeboom AR, Sau J, Bonmartin A. A model of the dual effect of gadopentetate dimeglumine on dynamic brain MR images. J Magn Reson Imaging 1999; 10:242–253.
50. Haselhorst R, Kappos L, Bilecen D, et al. Dynamic susceptibility contrast MR imaging of plaque development in multiple sclerosis: application of an extended blood-brain barrier leakage correction. J Magn Reson Imaging 2000;11:495–505.
51. Hou L, Yang Y, Mattay VS, Frank JA, Duyn JH. Optimization of fast acquisition methods for whole-brain relative cerebral blood volume (rCBV) mapping with susceptibility contrast agents. J Magn Reson Imaging 1999;9:233–239.
52. Moseley ME, Vexler Z, Asgari HS, et al. Comparison of Gd- and Dy-chelates for T2 contrast-enhanced imaging. Magn Reson Med 1991;22:259–264.
53. Lev MH, Kulke SF, Sorensen AG, et al. Contrast-to-noise ratio in functional MRI of relative cerebral blood volume with sprodiamide injection. J Magn Reson Imaging 1997;7:523–527.
54. De La Paz RL, Ott IL, Paola T. Recurrent brain tumour versus radiation necrosis: comparison of MR relative cerebral blood volume maps and FDG-PET. Radiology 1995;197(P):169.
55. Forsting M, Reith W, Dorfler A, von Kummer R, Hacke W, Sartor K. MRI in acute cerebral ischaemia: perfusion imaging with superparamagnetic iron oxide in a rat model. Neuroradiology 1994;36: 23–26.
56. Bjornerud A, Johansson LO, Ahlstrom HK. Renal T(*)(2) perfusion using an iron oxide nanoparticle contrast agent-influence of T(1) relaxation on the first-pass response. Magn Reson Med 2002;47: 298–304.
57. Reimer P, Schuierer G, Balzer T, Peters PE. Application of a superparamagnetic iron oxide (Resovist) for MR imaging of human cerebral blood volume. Magn Reson Med 1995;34:694–697.
58. Bjerner T, Johansson L, Ericsson A, Wikstrom G, Hemmingsson A, Ahlstrom H. First-pass myocardial perfusion MR imaging with outer-volume suppression and the intravascular contrast agent NC100150 injection: preliminary results in eight patients. Radiology 2001;221:822–826.
59. Ichikawa T, Haradome H, Hachiya J, Nitatori T, Araki T. Characterization of hepatic lesions by perfusion-weighted MR imaging with an echoplanar sequence. AJR Am J Roentgenol 1998;170: 1029–1034.
60. Ichikawa T, Arbab AS, Araki T, et al. Perfusion MR imaging with a superparamagnetic iron oxide using T2-weighted and susceptibility-sensitive echoplanar sequences: evaluation of tumor vascularity in hepatocellular carcinoma. AJR Am J Roentgenol 1999;173: 207–213.
61. Kuhl CK, Bieling H, Gieseke J, et al. Breast neoplasms: T2* susceptibility-contrast, first-pass perfusion MR imaging. Radiology 1997;202:87–95.
62. Kvistad KA, Lundgren S, Fjosne HE, Smenes E, Smethurst HB, Haraldseth O. Differentiating benign and malignant breast lesions with T2*-weighted first pass perfusion imaging. Acta Radiol 1999; 40:45–51.
63. Weind KL, Maier CF, Rutt BK, Moussa M. Invasive carcinomas and fibroadenomas of the breast: comparison of microvessel distributions—implications for imaging modalities. Radiology 1998; 208:477–483.
64. Jitsuiki Y, Hasebe T, Tsuda H, et al. Optimizing microvessel counts according to tumor zone in invasive ductal carcinoma of the breast. Mod Pathol 1999;12:492–498.
65. Buadu LD, Murakami J, Murayama S, et al. Breast lesions: correlation of contrast medium enhancement patterns on MR images with histopathologic findings and tumor angiogenesis. Radiology 1996;200:639–649.
66. Hacklander T, Reichenbach JR, Modder U. Comparison of cerebral blood volume measurements using the T1 and T2* methods in normal human brains and brain tumors. J Comput Assist Tomogr 1997;21:857–866.
67. Cha S, Lu S, Johnson G, Knopp EA. Dynamic susceptibility contrast MR imaging: correlation of signal intensity changes with cerebral blood volume measurements. J Magn Reson Imaging 2000;11:114–119.
68. Maeda M, Itoh S, Kimura H, et al. Tumor vascularity in the brain: evaluation with dynamic susceptibility-contrast MR imaging. Radiology 1993;189:233–238.
69. Reith W, Heiland S, Erb G, Benner T, Forsting M, Sartor K. Dynamic contrast-enhanced T2*-weighted MRI in patients with cerebrovascular disease. Neuroradiology 1997;39:250–257.
70. Aronen HJ, Gazit IE, Louis DN, et al. Cerebral blood volume maps of gliomas: comparison with tumor grade and histologic findings. Radiology 1994;191:41–51.
71. Siegal T, Rubinstein R, Tzuk-Shina T, Gomori JM. Utility of relative cerebral blood volume mapping derived from perfusion magnetic resonance imaging in the routine follow up of brain tumors. J Neurosurg 1997;86:22–27.
72. Sugahara T, Korogi Y, Shigematsu Y, et al. Value of dynamic susceptibility contrast magnetic resonance imaging in the evaluation of intracranial tumors. Top Magn Reson Imaging 1999;10: 114–124.
73. Ostergaard L, Hochberg FH, Rabinov JD, et al. Early changes measured by magnetic resonance imaging in cerebral blood flow, blood volume, and blood-brain barrier permeability following dexamethasone treatment in patients with brain tumors. J Neurosurg 1999;90:300–305.

74. Sorensen AG, Copen WA, Ostergaard L, et al. Hyperacute stroke: simultaneous measurement of relative cerebral blood volume, relative cerebral blood flow, and mean tissue transit time. Radiology 1999;210:519–527.
75. Kleihues P, Burger PC, Scheithauer BW. The new WHO classification of brain tumours. Brain Pathol 1993;3:255–268.
76. Burger PC, Vogel FS, Green SB, Strike TA. Glioblastoma multiforme and anaplastic astrocytoma. Pathologic criteria and prognostic implications. Cancer 1985;56:1106–1111.
77. Sugahara T, Korogi Y, Kochi M, et al. Correlation of MR imaging-determined cerebral blood volume maps with histologic and angiographic determination of vascularity of gliomas. AJR Am J Roentgenol 1998;171:1479–1486.
78. Aronen HJ, Glass J, Pardo FS, et al. Echo-planar MR cerebral blood volume mapping of gliomas. Clinical utility. Acta Radiol 1995;36:520–528.
79. Knopp EA, Cha S, Johnson G, et al. Glial neoplasms: dynamic contrast-enhanced T2*-weighted MR imaging. Radiology 1999; 211:791–798.
80. Bagley LJ, Grossman RI, Judy KD, et al. Gliomas: correlation of magnetic susceptibility artifact with histologic grade. Radiology 1997;202:511–516.
81. Coffey RJ, Lunsford LD, Taylor FH. Survival after stereotactic biopsy of malignant gliomas. Neurosurgery 1988;22:465–473.
82. Fuss M, Wenz F, Essig M, et al. Tumor angiogenesis of low-grade astrocytomas measured by dynamic susceptibility contrast-enhanced MRI (DSC-MRI) is predictive of local tumor control after radiation therapy. Int J Radiat Oncol Biol Phys 2001;51:478–482.
83. Fuss M, Wenz F, Scholdei R, et al. Radiation-induced regional cerebral blood volume (rCBV) changes in normal brain and low-grade astrocytomas: quantification and time and dose-dependent occurrence. Int J Radiat Oncol Biol Phys 2000;48:53–58.
84. Cha S, Knopp EA, Johnson G, et al. Dynamic contrast-enhanced T2-weighted MR imaging of recurrent malignant gliomas treated with thalidomide and carboplatin. AJNR Am J Neuroradiol 2000; 21:881–890.
85. Roberts TP. Physiologic measurements by contrast-enhanced MR imaging: expectations and limitations. J Magn Reson Imaging 1997;7:82–90.
86. Evelhoch JL. Key factors in the acquisition of contrast kinetic data for oncology. J Magn Reson Imaging 1999;10:254–259.
87. Larsson HB, Stubgaard M, Frederiksen JL, Jensen M, Henriksen O, Paulson OB. Quantitation of blood-brain barrier defect by magnetic resonance imaging and gadolinium-DTPA in patients with multiple sclerosis and brain tumors. Magn Reson Med 1990;16: 117–131.
88. Gowland P, Mansfield P, Bullock P, Stehling M, Worthington B, Firth J. Dynamic studies of gadolinium uptake in brain tumors using inversion-recovery echo-planar imaging. Magn Reson Med 1992;26:241–258.
89. Parker GJ, Suckling J, Tanner SF, et al. Probing tumor microvascularity by measurement, analysis and display of contrast agent uptake kinetics. J Magn Reson Imaging 1997;7:564–574.
90. Brix G, Semmler W, Port R, Schad LR, Layer G, Lorenz WJ. Pharmacokinetic parameters in CNS Gd-DTPA enhanced MR imaging. J Comput Assist Tomogr 1991;15:621–628.
91. Hoffmann U, Brix G, Knopp MV, Hess T, Lorenz WJ. Pharmacokinetic mapping of the breast: a new method for dynamic MR mammography. Magn Reson Med 1995;33:506–514.
92. Buckley DL, Kerslake RW, Blackband SJ, Horsman A. Quantitative analysis of multi-slice Gd-DTPA enhanced dynamic MR images using an automated simplex minimization procedure. Magn Reson Med 1994;32:646–651.
93. Brookes JA, Redpath TW, Gilbert FJ, Needham G, Murray AD. Measurement of spin-lattice relaxation times with FLASH for dynamic MRI of the breast. Br J Radiol 1996;69:206–214.
94. Parker GJ, Baustert I, Tanner SF, Leach MO. Improving image quality and T(1) measurements using saturation recovery turbo-FLASH with an approximate K-space normalisation filter. Magn Reson Imaging 2000;18:157–167.
95. Donahue KM, Burstein D, Manning WJ, Gray ML. Studies of Gd-DTPA relaxivity and proton exchange rates in tissue. Magn Reson Med 1994;32:66–76.
96. Parker GJ, Suckling J, Tanner SF, Padhani AR, Husband JE, Leach MO. MRIW: parametric analysis software for contrast-enhanced dynamic MR imaging in cancer. Radiographics 1998;18: 497–506.
97. Flickinger FW, Allison JD, Sherry RM, Wright JC. Differentiation of benign from malignant breast masses by time-intensity evaluation of contrast enhanced MRI. Magn Reson Imaging 1993;11: 617–620.
98. Kaiser WA, Zeitler E. MR imaging of the breast: fast imaging sequences with and without Gd-DTPA. Preliminary observations. Radiology 1989;170:681–686.
99. Gribbestad IS, Nilsen G, Fjosne HE, Kvinnsland S, Haugen OA, Rinck PA. Comparative signal intensity measurements in dynamic gadolinium-enhanced MR mammography. J Magn Reson Imaging 1994;4:477–480.
100. Kuhl CK, Mielcareck P, Klaschik S, et al. Dynamic breast MR imaging: are signal intensity time course data useful for differential diagnosis of enhancing lesions? Radiology 1999;211:101–110.
101. Tofts PS. Modeling tracer kinetics in dynamic Gd-DTPA MR imaging. J Magn Reson Imaging 1997;7:91–101.
102. Tofts PS, Berkowitz B, Schnall MD. Quantitative analysis of dynamic Gd-DTPA enhancement in breast tumors using a permeability model. Magn Reson Med 1995;33:564–568.
103. den Boer JA, Hoenderop RK, Smink J, et al. Pharmacokinetic analysis of Gd-DTPA enhancement in dynamic three-dimensional MRI of breast lesions. J Magn Reson Imaging 1997;7:702–715.
104. Stomper PC, Winston JS, Herman S, Klippenstein DL, Arredondo MA, Blumenson LE. Angiogenesis and dynamic MR imaging gadolinium enhancement of malignant and benign breast lesions. Breast Cancer Res Treat 1997;45:39–46.
105. Weidner N. Tumour vascularity and proliferation: clear evidence of a close relationship. J Pathol 1999;189:297–299.
106. Hawighorst H, Knapstein PG, Weikel W, et al. Angiogenesis of uterine cervical carcinoma: characterization by pharmacokinetic magnetic resonance parameters and histological microvessel density with correlation to lymphatic involvement. Cancer Res 1997; 57:4777–4786.
107. Tynninen O, Aronen HJ, Ruhala M, et al. MRI enhancement and microvascular density in gliomas. Correlation with tumor cell proliferation. Invest Radiol 1999;34:427–434.
108. Buckley DL, Drew PJ, Mussurakis S, Monson JR, Horsman A. Microvessel density of invasive breast cancer assessed by dynamic Gd-DTPA enhanced MRI. J Magn Reson Imaging 1997;7: 461–464.
109. Hulka CA, Edmister WB, Smith BL, et al. Dynamic echo-planar imaging of the breast: experience in diagnosing breast carcinoma and correlation with tumor angiogenesis. Radiology 1997;205: 837–842.
110. Cooper RA, Carrington BM, Loncaster JA, et al. Tumour oxygenation levels correlate with dynamic contrast-enhanced magnetic resonance imaging parameters in carcinoma of the cervix. Radiother Oncol 2000;57:53–59.
111. Knopp MV, Weiss E, Sinn HP, et al. Pathophysiologic basis of contrast enhancement in breast tumors. J Magn Reson Imaging 1999;10:260–266.
112. Hawighorst H, Knapstein PG, Knopp MV, et al. Uterine cervical carcinoma: comparison of standard and pharmacokinetic analysis of time-intensity curves for assessment of tumor angiogenesis and patient survival. Cancer Res 1998;58:3598–3602.
113. Bhujwalla ZM, Artemov D, Natarajan K, Ackerstaff E, Solaiyappan M. Vascular differences detected by MRI for metastatic versus nonmetastatic breast and prostate cancer xenografts. Neoplasia 2001;3:143–153.
114. George ML, Dzik-Jurasz AS, Padhani AR, et al. Non-invasive methods of assessing angiogenesis and their value in predicting response to treatment in colorectal cancer. Br J Surg 2001;88: 1628–1636.
115. Pham CD, Roberts TP, van Bruggen N, et al. Magnetic resonance imaging detects suppression of tumor vascular permeability after administration of antibody to vascular endothelial growth factor. Cancer Invest 1998;16:225–230.
116. Thomas A, Morgan B, Drevs J, et al. Pharmacodynamic results using dynamic contrast enhanced magnetic resonance imaging, of 2 phase 1 studies of the VEGF inhibitor PTK787/ZK 222584 in patients with liver metastases from colorectal cancer. In: Proceedings of American Society of Clinical Oncology, San Francisco, 2001. p A279.
117. Yamashita Y, Baba T, Baba Y, et al. Dynamic contrast-enhanced MR imaging of uterine cervical cancer: pharmacokinetic analysis with histopathologic correlation and its importance in predicting the outcome of radiation therapy. Radiology 2000;216:803–809.

118. Lyng H, Vorren AO, Sundfor K, et al. Assessment of tumor oxygenation in human cervical carcinoma by use of dynamic Gd-DTPA-enhanced MR imaging. J Magn Reson Imaging 2001;14: 750–756.
119. Stoutjesdijk MJ, Boetes C, Jager GJ, et al. Magnetic resonance imaging and mammography in women with a hereditary risk of breast cancer. J Natl Cancer Inst 2001;93:1095–1102.
120. Brown J, Buckley D, Coulthard A, et al. Magnetic resonance imaging screening in women at genetic risk of breast cancer: imaging and analysis protocol for the UK multicentre study. UK MRI Breast Screening Study Advisory Group. Magn Reson Imaging 2000;18:765–776.
121. Kuhl CK, Schmutzler RK, Leutner CC, et al. Breast MR imaging screening in 192 women proved or suspected to be carriers of a breast cancer susceptibility gene: preliminary results. Radiology 2000;215:267–279.
122. Tilanus-Linthorst MM, Obdeijn IM, Bartels KC, de Koning HJ, Oudkerk M. First experiences in screening women at high risk for breast cancer with MR imaging. Breast Cancer Res Treat 2000; 63:53–60.
123. van der Woude HJ, Verstraete KL, Hogendoorn PC, Taminiau AH, Hermans J, Bloem JL. Musculoskeletal tumors: does fast dynamic contrast-enhanced subtraction MR imaging contribute to the characterization? Radiology 1998;208:821–828.
124. Boetes C, Barentsz JO, Mus RD, et al. MR characterization of suspicious breast lesions with a gadolinium-enhanced TurboFLASH subtraction technique. Radiology 1994;193:777–781.
125. Gilles R, Guinebretiere JM, Shapeero LG, et al. Assessment of breast cancer recurrence with contrast-enhanced subtraction MR imaging: preliminary results in 26 patients. Radiology 1993;188: 473–478.
126. Heywang SH, Wolf A, Pruss E, Hilbertz T, Eiermann W, Permanetter W. MR imaging of the breast with Gd-DTPA: use and limitations. Radiology 1989;171:95–103.
127. Stomper PC, Herman S, Klippenstein DL, et al. Suspect breast lesions: findings at dynamic gadolinium-enhanced MR imaging correlated with mammographic and pathologic features. Radiology 1995;197:387–395.
128. Fobben ES, Rubin CZ, Kalisher L, Dembner AG, Seltzer MH, Santoro EJ. Breast MR imaging with commercially available techniques: radiologic-pathologic correlation. Radiology 1995;196:143–152.
129. Brinck U, Fischer U, Korabiowska M, Jutrowski M, Schauer A, Grabbe E. The variability of fibroadenoma in contrast-enhanced dynamic MR mammography. AJR Am J Roentgenol 1997;168: 1331–1334.
130. Padhani AR, Gapinski CJ, Macvicar DA, et al. Dynamic contrast enhanced MRI of prostate cancer: correlation with morphology and tumour stage, histological grade and PSA. Clin Radiol 2000; 55:99–109.
131. Turnbull LW, Buckley DL, Turnbull LS, Liney GP, Knowles AJ. Differentiation of prostatic carcinoma and benign prostatic hyperplasia: correlation between dynamic Gd-DTPA-enhanced MR imaging and histopathology. J Magn Reson Imaging 1999;9:311–316.
132. Jager GJ, Ruijter ET, van de Kaa CA, et al. Dynamic TurboFLASH subtraction technique for contrast-enhanced MR imaging of the prostate: correlation with histopathologic results. Radiology 1997;203:645–652.
133. Liu PF, Krestin GP, Huch RA, Gohde SC, Caduff RF, Debatin JF. MRI of the uterus, uterine cervix, and vagina: diagnostic performance of dynamic contrast-enhanced fast multiplanar gradient-echo imaging in comparison with fast spin-echo T2-weighted pulse imaging. Eur Radiol 1998;8:1433–1440.
134. Barentsz JO, Jager GJ, van Vierzen PB, et al. Staging urinary bladder cancer after transurethral biopsy: value of fast dynamic contrast-enhanced MR imaging. Radiology 1996;201:185–193.
135. Huch Boni RA, Boner JA, Lutolf UM, Trinkler F, Pestalozzi DM, Krestin GP. Contrast-enhanced endorectal coil MRI in local staging of prostate carcinoma. J Comput Assist Tomogr 1995;19:232–237.
136. Barentsz JO, Berger-Hartog O, Witjes JA, et al. Evaluation of chemotherapy in advanced urinary bladder cancer with fast dynamic contrast-enhanced MR imaging. Radiology 1998;207:791–797.
137. Reddick WE, Taylor JS, Fletcher BD. Dynamic MR imaging (DEMRI) of microcirculation in bone sarcoma. J Magn Reson Imaging 1999;10:277–285.
138. van der Woude HJ, Bloem JL, Verstraete KL, Taminiau AH, Nooy MA, Hogendoorn PC. Osteosarcoma and Ewing's sarcoma after neoadjuvant chemotherapy: value of dynamic MR imaging in detecting viable tumor before surgery. Am J Roentgenol 1995;165: 593–598.
139. Padhani AR, MacVicar AD, Gapinski CJ, et al. Effects of androgen deprivation on prostatic morphology and vascular permeability evaluated with MR imaging. Radiology 2001;218:365–374.
140. Knopp MV, Brix G, Junkermann HJ, Sinn HP. MR mammography with pharmacokinetic mapping for monitoring of breast cancer treatment during neoadjuvant therapy. Magn Reson Imaging Clin N Am 1994;2:633–658.
141. Padhani AR, Hayes C, Assersohn L, Powles T, Leach MO, Husband JE. Response of breast carcinoma to chemotherapy—MR permeability changes using histogram analysis. In: Proceedings of the 8th Annual Meeting of ISMRM, Denver, 2000. p 2160.
142. Devries AF, Griebel J, Kremser C, et al. Tumor microcirculation evaluated by dynamic magnetic resonance imaging predicts therapy outcome for primary rectal carcinoma. Cancer Res 2001;61: 2513–2516.
143. de Vries A, Griebel J, Kremser C, et al. Monitoring of tumor microcirculation during fractionated radiation therapy in patients with rectal carcinoma: preliminary results and implications for therapy. Radiology 2000;217:385–391.
144. Mayr NA, Yuh WT, Arnholt JC, et al. Pixel analysis of MR perfusion imaging in predicting radiation therapy outcome in cervical cancer. J Magn Reson Imaging 2000;12:1027–1033.
145. Burn PR, McCall JM, Chinn RJ, Vashisht A, Smith JR, Healy JC. Uterine fibroleiomyoma: MR imaging appearances before and after embolization of uterine arteries. Radiology 2000;214:729–734.
146. Jha RC, Ascher SM, Imaoka I, Spies JB. Symptomatic fibroleiomyomata: MR imaging of the uterus before and after uterine arterial embolization. Radiology 2000;217:228–235.
147. Li W, Brophy DP, Chen Q, Edelman RR, Prasad PV. Semiquantitative assessment of uterine perfusion using first pass dynamic contrast-enhanced MR imaging for patients treated with uterine fibroid embolization. J Magn Reson Imaging 2000;12:1004–1008.
148. Padhani AR, O'Donell A, Hayes C, et al. Dynamic contrast enhanced MR imaging in the evaluation of antiangiogenesis therapy. In: Molecular Targets and Cancer Therapeutics: Discovery, Development and Cancer Therapeutics: The Joint AACR-NCI-EORTC Meeting, Washington, 1999, Clinical Cancer Research. p 3828S.
149. Galbraith SMLM, Taylor NJ, Maxwell R, et al. Combretastatin A4 phosphate reduces tumour blood flow in animal and man, demonstrated by MRI. In: Proceedings of American Society of Clinical Oncology, San Francisco, 2001. p A279.
150. Hawighorst H, Weikel W, Knapstein PG, et al. Angiogenic activity of cervical carcinoma: assessment by functional magnetic resonance imaging-based parameters and a histomorphological approach in correlation with disease outcome. Clin Cancer Res 1998;4:2305–2312.
151. Mayr NA, Yuh WT, Magnotta VA, et al. Tumor perfusion studies using fast magnetic resonance imaging technique in advanced cervical cancer: a new noninvasive predictive assay. Int J Radiat Oncol Biol Phys 1996;36:623–633.
152. Kerslake RW, Fox JN, Carleton PJ, et al. Dynamic contrast-enhanced and fat suppressed magnetic resonance imaging in suspected recurrent carcinoma of the breast: preliminary experience. Br J Radiol 1994;67:1158–1168.
153. Mussurakis S, Buckley DL, Bowsley SJ, et al. Dynamic contrast-enhanced magnetic resonance imaging of the breast combined with pharmacokinetic analysis of gadolinium-DTPA uptake in the diagnosis of local recurrence of early stage breast carcinoma. Invest Radiol 1995;30:650–662.
154. Kinkel K, Tardivon AA, Soyer P, et al. Dynamic contrast-enhanced subtraction versus T2-weighted spin-echo MR imaging in the follow-up of colorectal neoplasm: a prospective study of 41 patients. Radiology 1996;200:453–458.
155. Hawnaur JM, Zhu XP, Hutchinson CE. Quantitative dynamic contrast enhanced MRI of recurrent pelvic masses in patients treated for cancer. Br J Radiol 1998;71:1136–1142.
156. Dao TH, Rahmouni A, Campana F, Laurent M, Asselain B, Fourquet A. Tumor recurrence versus fibrosis in the irradiated breast: differentiation with dynamic gadolinium-enhanced MR imaging. Radiology 1993;187:751–755.

157. Heywang-Kobrunner SH, Schlegel A, Beck R, et al. Contrast-enhanced MRI of the breast after limited surgery and radiation therapy. J Comput Assist Tomogr 1993;17:891–900.
158. Blomqvist L, Fransson P, Hindmarsh T. The pelvis after surgery and radio-chemotherapy for rectal cancer studied with Gd-DTPA-enhanced fast dynamic MR imaging. Eur Radiol 1998;8:781–787.
159. Shames DM, Kuwatsuru R, Vexler V, Muhler A, Brasch RC. Measurement of capillary permeability to macromolecules by dynamic magnetic resonance imaging: a quantitative noninvasive technique. Magn Reson Med 1993;29:616–622.
160. Daldrup H, Shames DM, Wendland M, et al. Correlation of dynamic contrast-enhanced MR imaging with histologic tumor grade: comparison of macromolecular and small-molecular contrast media. AJR Am J Roentgenol 1998;171:941–949.
161. Ogan MD, Schmiedl U, Moseley ME, Grodd W, Paajanen H, Brasch RC. Albumin labeled with Gd-DTPA. An intravascular contrast-enhancing agent for magnetic resonance blood pool imaging: preparation and characterization. Invest Radiol 1987;22:665–671.
162. van Dijke CF, Brasch RC, Roberts TP, et al. Mammary carcinoma model: correlation of macromolecular contrast-enhanced MR imaging characterizations of tumor microvasculature and histologic capillary density. Radiology 1996;198:813–818.
163. Helbich TH, Roberts TP, Gossmann A, et al. Quantitative gadopentetate-enhanced MRI of breast tumors: testing of different analytic methods. Magn Reson Med 2000;44:915–924.
164. Roberts HC, Saeed M, Roberts TP, et al. Comparison of albumin-(Gd-DTPA)30 and Gd-DTPA-24-cascade-polymer for measurements of normal and abnormal microvascular permeability. J Magn Reson Imaging 1997;7:331–338.
165. Adam G, Muhler A, Spuntrup E, et al. Differentiation of spontaneous canine breast tumors using dynamic magnetic resonance imaging with 24-gadolinium-DTPA-cascade-polymer, a new blood-pool agent. Preliminary experience. Invest Radiol 1996;31: 267–274.
166. Su MY, Wang Z, Carpenter PM, Lao X, Muhler A, Nalcioglu O. Characterization of N-ethyl-N-nitrosourea-induced malignant and benign breast tumors in rats by using three MR contrast agents. J Magn Reson Imaging 1999;9:177–186.
167. Evelhoch J, Brown T, Chenevert T, et al. Consensus recommendation for acquisition of dynamic contrast-enhanced MRI data in oncology. In: Proceedings of the 8th Annual Meeting of ISMRM, Denver, 2000. p 1439.
168. Heywang-Kobrunner SH, Haustein J, Pohl C, et al. Contrast-enhanced MR imaging of the breast: comparison of two different doses of gadopentetate dimeglumine. Radiology 1994;191:639–646.
169. Tofts PS, Kermode AG. Measurement of the blood-brain barrier permeability and leakage space using dynamic MR imaging. 1. Fundamental concepts. Magn Reson Med 1991;17:357–367.
170. Henderson E, Rutt BK, Lee TY. Temporal sampling requirements for the tracer kinetics modeling of breast disease. Magn Reson Imaging 1998;16:1057–1073.
171. Tofts PS, Berkowitz BA. Measurement of capillary permeability from the Gd enhancement curve: a comparison of bolus and constant infusion injection methods. Magn Reson Imaging 1994; 12:81–91.
172. Noseworthy MD, Sussman MS, Haider M, Baruchel S. Dynamic contrast enhanced liver MRI using a motion tracking algorithm. In: Proceedings of the 9th Annual Meeting of ISMRM, Glasgow, Scotland, 2001. p 2240.
173. Port RE, Knopp MV, Hoffmann U, Milker-Zabel S, Brix G. Multicompartment analysis of gadolinium chelate kinetics: blood-tissue exchange in mammary tumors as monitored by dynamic MR imaging. J Magn Reson Imaging 1999;10:233–241.
174. Bland JM, Altman DG. Measurement error. BMJ 1996;313:744.
175. Bland JM, Altman DG. Measurement error proportional to the mean. BMJ 1996;313:106.
176. Bland JM, Altman DG. Measurement error and correlation coefficients. BMJ 1996;313:41–42.
177. Jackson A, Kassner A, Zhu XP, Li KL. Reproducibility of T2* blood volume and vascular tortuosity maps in cerebral gliomas. J Magn Reson Imaging 2001;14:510–516.
178. Galbraith SM, Lodge MA, Taylor NJ, et al. Reproducibility of dynamic contrast enhanced MRI in human muscle and tumours: comparison of quantitative and semi-quantitative analysis. NMR Biomed 2002;15:132–142.
179. Padhani AR, Hayes C, Landau S, Leach MO. Reproducibility of quantitative dynamic MRI of normal human tissues. NMR Biomed 2002;15:143–154.
180. Evelhoch J, LoRusso P, Latif Z, et al. Reproducibility of dynamic contrast-enhanced (DCE-MRI) assessment of tumor vascularity. In: American Society of Clinical Oncology Annual Meeting, San Francisco, 2001. p 399.
181. Rijpkema M, Kaanders JH, Joosten FB, van der Kogel AJ, Heerschap A. Method for quantitative mapping of dynamic MRI contrast agent uptake in human tumors. J Magn Reson Imaging 2001;14:457–463.
182. Buckley DL, Manton DJ. Potential problem that may influence the quantitative analysis of dynamically acquired contrast-enhanced magnetic resonance images. Magn Reson Imaging 1999;17:319–320.
183. Eberhard A, Kahlert S, Goede V, Hemmerlein B, Plate KH, Augustin HG. Heterogeneity of angiogenesis and blood vessel maturation in human tumors: implications for antiangiogenic tumor therapies. Cancer Res 2000;60:1388–1393.
184. Fuentes MA, Keith CJ, Griffiths M, Durbridge G, Miles KA. Hepatic haemodynamics: interrelationships between contrast enhancement and perfusion on CT and Doppler perfusion indices. Br J Radiol 2002;75:17–23.
185. Miles KA, Griffiths MR, Fuentes MA. Standardized perfusion value: universal CT contrast enhancement scale that correlates with FDG PET in lung nodules. Radiology 2001;220:548–553.
186. Gillard JH, Minhas PS, Hayball MP, et al. Assessment of quantitative computed tomographic cerebral perfusion imaging with H2(15)O positron emission tomography. Neurol Res 2000;22:457–464.
187. Maxwell RJ, Wilson J, Prise VE, et al. Evaluation of the antivascular effects of combretastatin in rodent tumours by dynamic contrast enhanced MRI. NMR Biomed 2002;15:89–98.
188. Hayes C, Padhani AR, Leach MO. Assessing changes in tumour vascular function using dynamic contrast-enhanced magnetic resonance imaging. NMR Biomed 2002;15:154–163.
189. Liney GP, Gibbs P, Hayes C, Leach MO, Turnbull LW. Dynamic contrast-enhanced MRI in the differentiation of breast tumors: user-defined versus semi-automated region-of-interest analysis. J Magn Reson Imaging 1999;10:945–949.
190. Roberts HC, Roberts TP, Brasch RC, Dillon WP. Quantitative measurement of microvascular permeability in human brain tumors achieved using dynamic contrast-enhanced MR imaging: correlation with histologic grade. AJNR Am J Neuroradiol 2000; 21:891–899.
191. Ludemann L, Grieger W, Wurm R, Budzisch M, Hamm B, Zimmer C. Comparison of dynamic contrast-enhanced MRI with WHO tumor grading for gliomas. Eur Radiol 2001;11:1231–1241.
192. Zhu XP, Li KL, Kamaly-Asl ID, et al. Quantification of endothelial permeability, leakage space, and blood volume in brain tumors using combined T1 and T2* contrast-enhanced dynamic MR imaging. J Magn Reson Imaging 2000;11:575–585.
193. Fischer U, Kopka L, Grabbe E. Breast carcinoma: effect of preoperative contrast-enhanced MR imaging on the therapeutic approach. Radiology 1999;213:881–888.
194. Mumtaz H, Davidson T, Hall-Craggs MA, et al. Comparison of magnetic resonance imaging and conventional triple assessment in locally recurrent breast cancer. Br J Surg 1997;84:1147–1151.
195. Padhani AR, Neeman M. Challenges for imaging angiogenesis. Br J Radiol 2001;74:886–890.
196. Tatum JL, Hoffman JM. Role of imaging in clinical trials of antiangiogenesis therapy in oncology. Acad Radiol 2000;7:798–799.
197. Ikeda O, Yamashita Y, Takahashi M. Gd-enhanced dynamic magnetic resonance imaging of breast masses. Top Magn Reson Imaging 1999;10:143–151.